

A Highly Reliable Copper Nanowire/Nanoparticle Ink Pattern with High Conductivity on Flexible Substrate Prepared via a Flash Light-Sintering Technique

Sung-Jun Joo,[§] Sung-Hyeon Park,[§] Chang-Jin Moon,[§] and Hak-Sung Kim^{*,§,‡}

[§]Department of Mechanical Convergence Engineering, Hanyang University, Haengdang-dong, Seongdong-gu, Seoul 133-791, South Korea

[‡]Institute of Nano Science and Technology, Hanyang University, Seoul, 133-791, Korea

ABSTRACT: In this work, copper nanowires (NWs) and Cu nanoparticles (NPs) were employed to increase the reliability of a printed electrode pattern under mechanical bending fatigue. The fabricated Cu NW/NP inks with different weight fractions of Cu NWs were printed on a polyimide substrate and flash light-sintered within a few milliseconds at room temperature under ambient conditions. Then, 1000 cycles of outer and inner bending fatigue tests were performed using a lab-made fatigue tester. The flash light-sintered Cu NW/NP ink film with 5 wt % Cu NWs prepared under the flash light-sintering conditions (12.5 J·cm⁻² irradiation energy, 10 ms pulse duration, and one pulse) showed a lower resistivity (22.77 μΩ·cm) than those of the only Cu NPs and Cu NWs ink (94.01 μΩ·cm and 104.15 μΩ·cm, respectively). In addition, the resistance change ($\Delta R \cdot R_0^{-1}$) of the 5 wt % Cu NWs Cu NW/NP film was greatly enhanced to 4.19 compared to the 92.75 of the Cu NPs film obtained under mechanical fatigue conditions over 1000 cycles and an outer bending radius of 7 mm. These results were obtained by the densification and enhanced mechanical flexibility of flash light-sintered Cu NW/NP network, which resulted in prevention of crack initiation and propagation. To characterize the Cu NW/NP ink film, X-ray diffraction and scanning electron microscopy were used.

KEYWORDS: flash light sintering, copper nanoparticles, copper nanowires, printed electronics, reliability of electrode



INTRODUCTION

The direct printing of conductive materials has received much attention over the past few decades due to its simplicity, efficiency of material usage, scalability, and flexibility.^{1–3} Owing to these benefits, this process has been utilized in various applications such as flexible displays, organic solar cells, wearable displays, and flexible batteries.^{4–6} Additionally, direct printing technology can be combined with roll-to-roll (R2R) and inkjet printing for mass production and precise patterning as promising candidates to replace conventional lithography processes.

For the printing materials, solution-based noble metallic nanoparticle (NP) inks (Au, Ag, etc.) with an organic binder are widely employed in the sintering process on flexible polymer substrates.^{7,8} However, the commercialization of these noble metallic NPs is limited by its great expense. For this reason, copper (Cu) NPs have been recently proposed as an alternative due to their high electrical conductivity and low cost.^{9–11}

However, it is difficult to sinter Cu NPs because they are easily oxidized.¹² Also, the oxide shells of Cu NPs are difficult to be eliminated under ambient conditions using conventional sintering methods including conventional thermal sintering, plasma sintering, microwave sintering, and laser sintering.^{13–15}

Therefore, the flash light-sintering method with poly(*N*-vinylpyrrolidone) (PVP)-coated Cu NPs has been developed because the oxide shells of the Cu NPs can be eliminated in a few milliseconds by the combined functions of flash light and PVP evaporation at room temperature under ambient conditions.^{16–19}

Moreover, flexible electrical devices should maintain their electrical performances under severe conditions such as

Received: October 2, 2014

Accepted: February 25, 2015

Published: February 25, 2015

Table 1. Contents of Formulated Cu NW/NP Ink

DEG (g)	PVP (g)	Cu NPs (wt %)	Cu NWs (wt %)	total Cu (g)
9	0.9	100	0	11.4
9	0.9	99	1	11.4
9	0.9	97	3	11.4
9	0.9	95	5	11.4
9	0.9	0	100	11.4

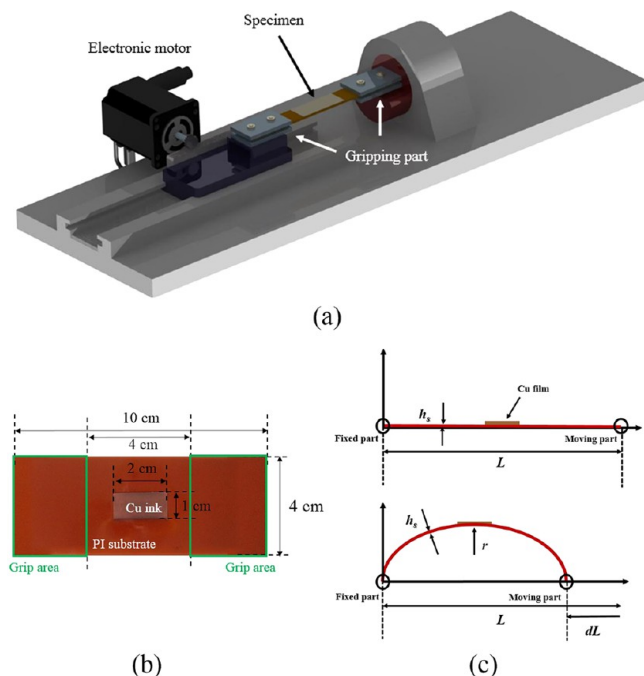


Figure 1. Schematics of (a) the bending fatigue tester, (b) the photograph of flash light-sintered Cu NW/NP ink for the fatigue test, and (c) bending radius calculation.

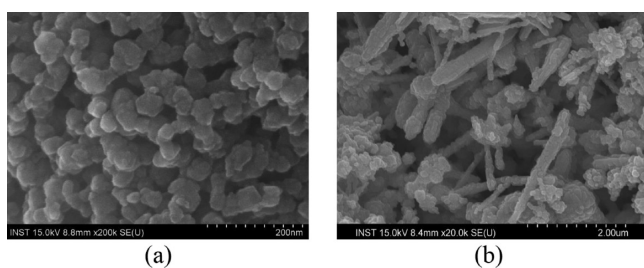


Figure 2. SEM images of unsintered (a) Cu NPs and (b) Cu NWs used in this work.

mechanical bending, twisting, and stretching.^{20,21} However, the sintered metallic NPs film showed the strain of fracture (ϵ_f) even in small elongation, resulting in brittle failure induced by highly concentrated stress at the necklike junction as reported by Siow et al.²² Also, there are several works reported about nanocrystalline Cu: for the grain size <25 nm and the ductility <2% elongation, whereas the bulk Cu has large ductility, up to 40–70% elongation.^{23,24} Therefore, it is difficult to utilize the sintered metallic NP (Ag, Au, Cu, etc.) films in flexible electronics applications subjected to repeated bending conditions. To overcome this limitation, several investigations have been conducted to increase the reliability of sintered metallic NPs thin films by mixing various materials such as carbon nanotubes, graphene, and nanowires (NWs).^{25–27} In general,

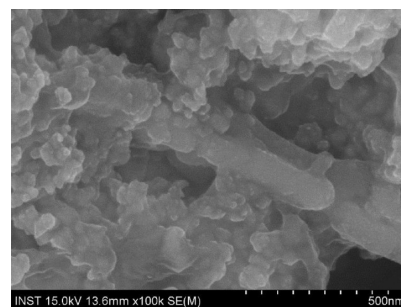


Figure 3. Morphology of Cu NW/NP ink after 24 h of ball-milling process.

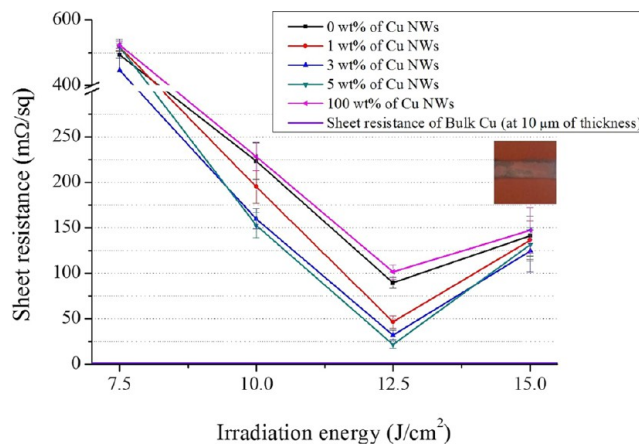


Figure 4. Sheet resistance of flash light-sintered Cu NW/NP-ink film with respect to the flash light-irradiation energy and weight fractions of Cu NWs. (inset) The damaged specimen at 15 J·cm⁻² irradiation energy (pulse duration: 10 ms, pulse number: 1).

Table 2. Summary of the Reported Light-Assisted Sintering of Similar Size of Cu NPs with Respect to Optimized Irradiation Condition, Substrate, and Conductivity

substrate	pulse number	pulse duration	optimized irradiation condition		
			irradiation energy	conductivity	author
PI	1	10 ms	12.5 J·cm ⁻²	72 mΩ/sq	Hwang ¹⁹
PI	1	10 ms	12.0 J·cm ⁻²		Park ³³
PI	1	10 ms	12.5 J·cm ⁻²	80 μΩ·cm	Joo ³⁴
PI	1	10 ms	12.5 J·cm ⁻²	54 μΩ·cm	Kim ³⁵

behaviors of metallic nanostructures such as electrodes fabricated by printed electronics under tensile and compressive loading conditions are not exactly same.²⁸ Therefore, mechanical characteristics of Cu film under tensile and compressive loading conditions must be investigated.

In this study, Cu NWs were added to a Cu NP ink to improve the electrical conductivity and reliability under repeatable mechanical fatigue in tension and compression conditions. Cu NW/NP inks with different weight fractions (wt %) of Cu NWs were printed onto a polyimide (PI) substrate and sintered by flash light irradiation. The viscosity of the fabricated Cu NW/NP ink was measured by using a viscometer. The sheet resistances of the sintered Cu NW/NP ink films were measured using a four-probe method with a source meter. For the resistivity calculations, two-dimensional profile imaging of the Cu NW/NP ink films was performed using an α step to measure the film thickness. Also, the flash light-sintered Cu NW/NP ink films

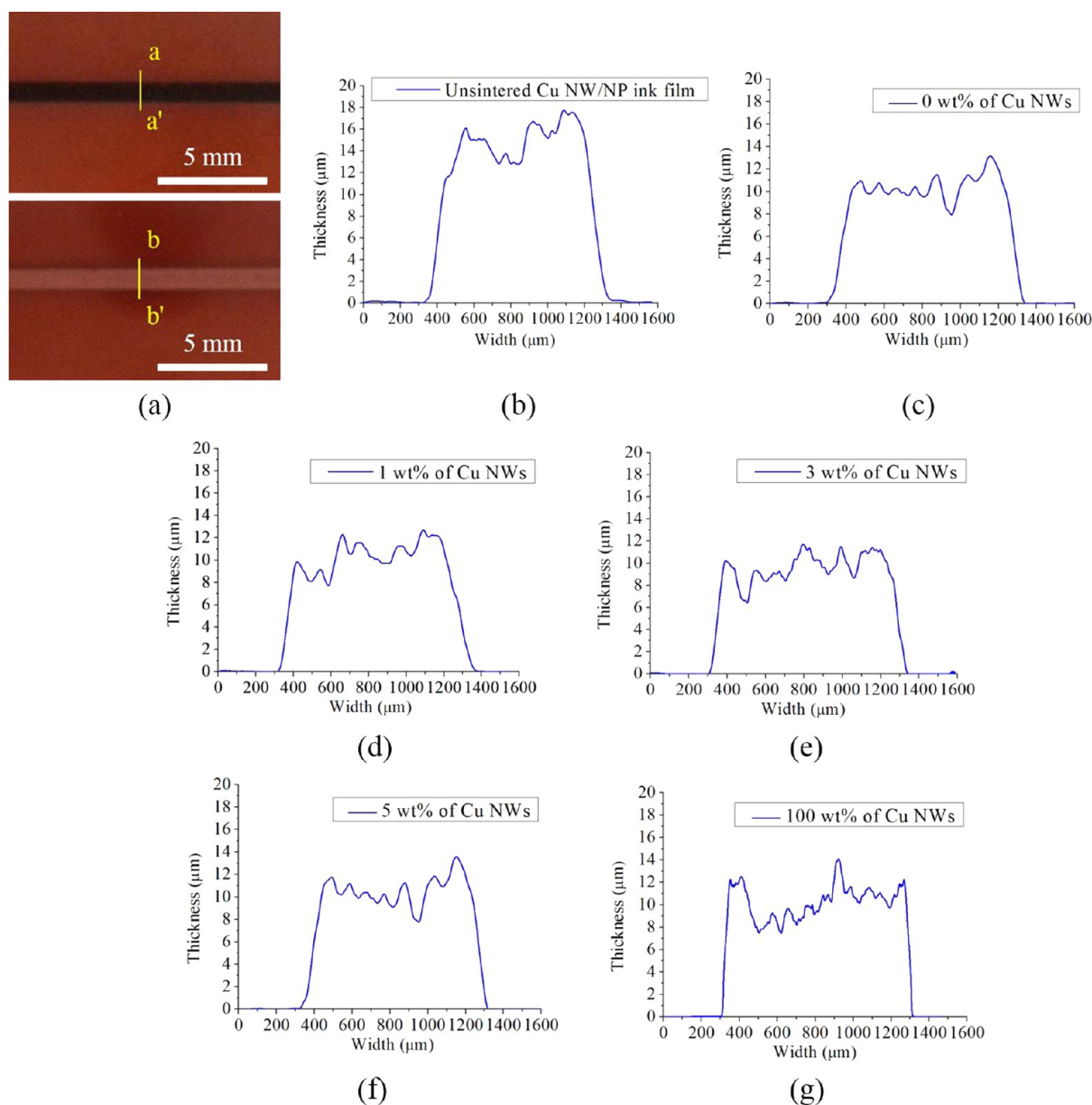


Figure 5. Photograph images of (a) printed (upper) and flash light-sintered (lower) Cu NW/NP ink film on PI substrate. Surface profiles of Cu NW/NP ink film with respect to wt % of Cu NWs: (b) the printed Cu NW/NP ink film and the flash light-sintered Cu NW/NP ink film with (c) 0, (d) 1, (e) 3, (f) 5, and (g) 100 wt % of Cu NWs (irradiation energy: $12.5 \text{ J}\cdot\text{cm}^{-2}$, pulse duration: 10 ms, pulse number: 1).

Table 3. Resistivity of Optimally Flash Light-Sintered Cu NW/NP-Ink with Five Different Weight Fractions of Cu NWs (pulse number: 1, pulse duration: 10 ms)

Cu NPs (wt %)	Cu NWs (wt %)	energy ($\text{J}\cdot\text{cm}^{-2}$)	resistivity ($\mu\Omega \text{ cm}$)	the times compared to bulk Cu ($1.77 \mu\Omega \text{ cm}$)
100	0	12.5	94.01 ± 6.31	53.12 ± 3.57
99	1	12.5	48.52 ± 7.30	27.42 ± 4.13
97	3	12.5	33.40 ± 5.19	18.87 ± 2.93
95	5	12.5	22.77 ± 4.24	12.87 ± 2.40
0	100	12.5	104.15 ± 7.92	58.84 ± 4.47

were characterized using microscopic and diffraction techniques including scanning electron microscopy (SEM) and X-ray diffraction (XRD). The reliability of the flash light-sintered Cu NW/NP ink films was investigated by measuring the resistance change during 1000 cycles of outer and inner bending tests as a function of the bending radius.

EXPERIMENTAL SECTION

Material Preparation and Fabrication of the Cu NW/NP Ink Film. For the fabrication of the Cu NW/NP inks, Cu NWs ($150 \pm 50 \text{ nm}$ in diameter, $1\text{--}2 \mu\text{m}$ in length, oxidized; SkySpring Nanomaterials, Inc.) and Cu NPs ($20\text{--}50 \text{ nm}$ in diameter, oxide thickness $>2 \text{ nm}$; Quantum Sphere Inc.) were dispersed in a mixed solvent containing 9 g of diethylene glycol (DEG, $\geq 99\%$; Sigma-Aldrich) and 0.9 g of PVP (MW 55 000; Sigma-Aldrich; see Table 1). For the premixing processes, the mixed Cu NW/NP inks were dispersed using an ultrasonicator and a mechanical stirrer for 2 h followed by ball milling for 24 h. The dispersed Cu NW/NP inks were entirely dispersed again using a three-roll milling process three times. To determine the optimal ratio of the Cu NW/NP inks, the wt % of Cu NWs was varied from 0 to 100 wt %, as shown in Table 1. The fabricated Cu NW/NP inks were pasted onto a PI substrate using a doctor blading method and dried on a hot plate (HSD 180, Misung Scientific Co.) at $100 \text{ }^\circ\text{C}$ for 30 min.

Flash Light-Sintering of the Cu NW/NP Ink Films. To sinter the Cu NW/NP ink films on PI substrates, flash light irradiation from a

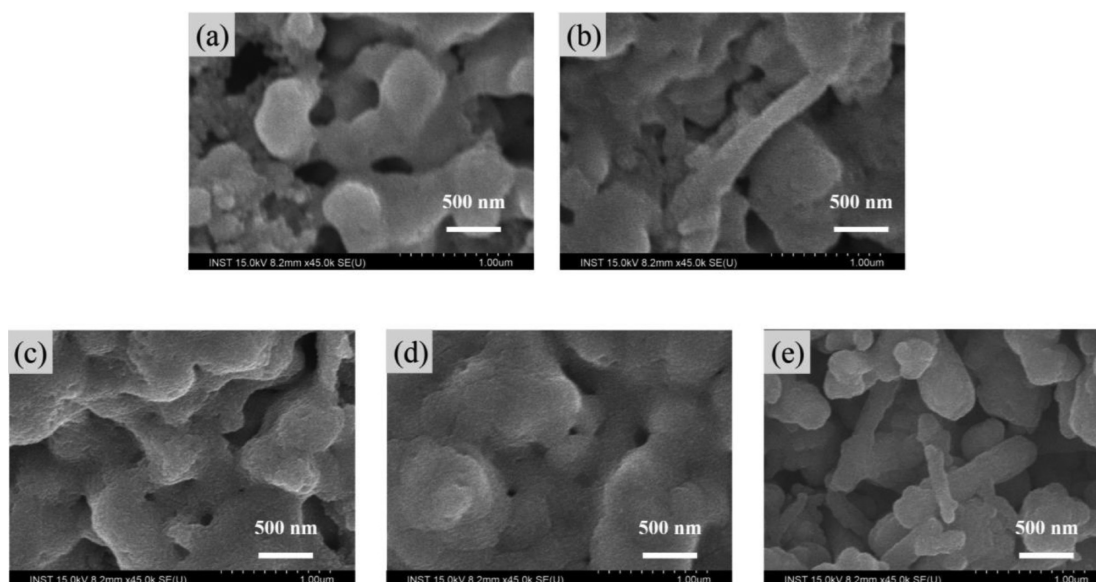


Figure 6. SEM images of flash light-sintered Cu NW/NP ink film at ca. (a) 0, (b) 1, (c) 3, (d) 5, and (e) 100 wt % of Cu NWs (irradiation energy: $12.5 \text{ J}\cdot\text{cm}^{-2}$, pulse duration: 10 ms, pulse number: 1).

xenon flash lamp (PerkinElmer Co.) was applied. The wavelengths of the xenon flash lamp ranged from 300 to 950 nm.^{19,29} The total applied energy varied from 7.5 to $15 \text{ J}\cdot\text{cm}^{-2}$ using one pulse with a 10 ms duration.

Mechanical Reliability of the Flash Light-Sintered Cu NW/NP Ink Films. The mechanical reliability of the sintered Cu NW/NP ink films was investigated under repeated tensile (outer bending) and compressive (inner bending) loading tests. For the reliability test, a lab-made bending tester was used, as shown in Figure 1a. The bending tester consists of a gripping part to fix the Cu NW/NP ink films on the PI substrate and a moving part to bend the Cu NW/NP ink films using an electronic motor.

For the fatigue test, a $2 \times 1 \text{ cm}$ sample of the Cu NW/NP ink was printed onto a $10 \times 4 \text{ cm}$ PI film (Figure 1b). The fatigue tests were conducted at a frequency of 1 Hz, and the two-point probe method was used to measure the resistance changes every 100 cycles for 1000 cycles.

In the fatigue test, the moving distances (d_t) were varied using the relationship in the following equation to generate three different bending radii (r) of 7, 10, and 15 mm, as shown in the schematic in Figure 1c.^{30,31} In eq 1, L is the substrate length (4 cm), and h_s is the thickness of the substrate ($225 \mu\text{m}$).

$$r = L \cdot [(d_t \cdot L^{-1}) - \{\pi h_s^2 \cdot (12L)^{-2}\}]^{-0.5} \quad (1)$$

Characterization. The viscosity of Cu NW/NP inks was measured using a viscometer (viscometer; SV-10, A&D Company). The surface and cross-section morphologies of the Cu NW/NP ink films were analyzed using an SEM (S4800 Hitachi). From the low-resolution SEM images, the average porosity of flash light-sintered Cu NW/NP ink films was calculated using MATLAB-based image analysis program (MathWorks Inc., USA). Crystal phase analysis of the flash light-sintered Cu NW/NP ink films was performed using a XRD (D/MAX RINT 2000, Rigaku). The sheet resistances of the sintered Cu NW/NP ink films were measured using a four-point probe (diameter of probe tip: $1 \mu\text{m}$, interval of probe tips: 1 mm; Modusystems, Inc.) with a source meter (2015 THD, Keithley). The film thicknesses of the Cu NW/NP ink films were measured using an α step (KLA Tencor AS500, Tencor instruments).

RESULTS AND DISCUSSION

Figure 2 shows the SEM images of Cu NPs and Cu NWs used in this work. The Cu NPs have spherical shape with an average diameter of $\sim 40 \text{ nm}$. Meanwhile, the Cu NWs were in the range

of $150 \pm 50 \text{ nm}$ in diameter and $1\text{--}2 \mu\text{m}$ in length with some broken NWs.

Figure 3 shows the surface morphology of Cu NW/NP ink after ball-milling process. With the long time premixing process, Cu NWs were dispersed between Cu NPs with some of the aggregates. Then, the dispersed Cu NW/NP inks were entirely dispersed using three-roll mill, having the grinding effect that diffused small aggregates of Cu NW/NP inks. These dispersion procedures contributed to the uniform distribution of Cu NPs and NWs after printing process. As a result, a small standard deviation with low sheet resistance of film was obtained after sintering process (sheet resistance and standard deviation in Figure 4).³² After dispersion process, the fabricated Cu NW/NP inks showed similar viscosity of $\sim 310\text{--}320$ centistokes.

To investigate the sintering characteristics of Cu NW/NP ink films, the flash light-irradiation energy was varied from 7.5 to $15 \text{ J}\cdot\text{cm}^{-2}$ with one pulse and 10 ms duration. The sheet resistances of Cu NW/NP ink films were measured with respect to the flash light irradiation conditions as shown in Figure 4. When the flash light irradiated, the oxide shells of Cu NPs and Cu NWs were removed by the intermediate alcohol from decomposed PVP, and necklike junctions among the Cu NW/NP were formed during flash light irradiation.¹⁶ In addition, the sheet resistance of the Cu NW/NP ink films gradually decreased as the irradiation light energy increased to $12.5 \text{ J}\cdot\text{cm}^{-2}$ because necklike junctions grew larger as the irradiation light energy increased.^{19,33} However, the sheet resistance of the $15 \text{ J}\cdot\text{cm}^{-2}$ flash light-irradiated Cu NW/NP ink films suddenly increased because it was damaged by the excess irradiation energy, as shown in the inset image in Figure 4. Accordingly, an irradiation energy of $12.5 \text{ J}\cdot\text{cm}^{-2}$ with one pulse and a 10 ms duration seemed to be the optimal flash light sintering condition for all of the Cu NW wt % specimens. The flash light sintering condition of $12.5 \text{ J}\cdot\text{cm}^{-2}$ energy and 10 ms duration was a similar condition in comparison with our previous works, which used the same Cu NPs^{19,33–35} (Table 2). Also, Park et al. investigated the temperature changes of Cu NPs film during flash light-sintering process; when the flash light irradiated with $12 \text{ J}\cdot\text{cm}^{-2}$ of energy, the maximum temperature of the Cu NPs film was increased to

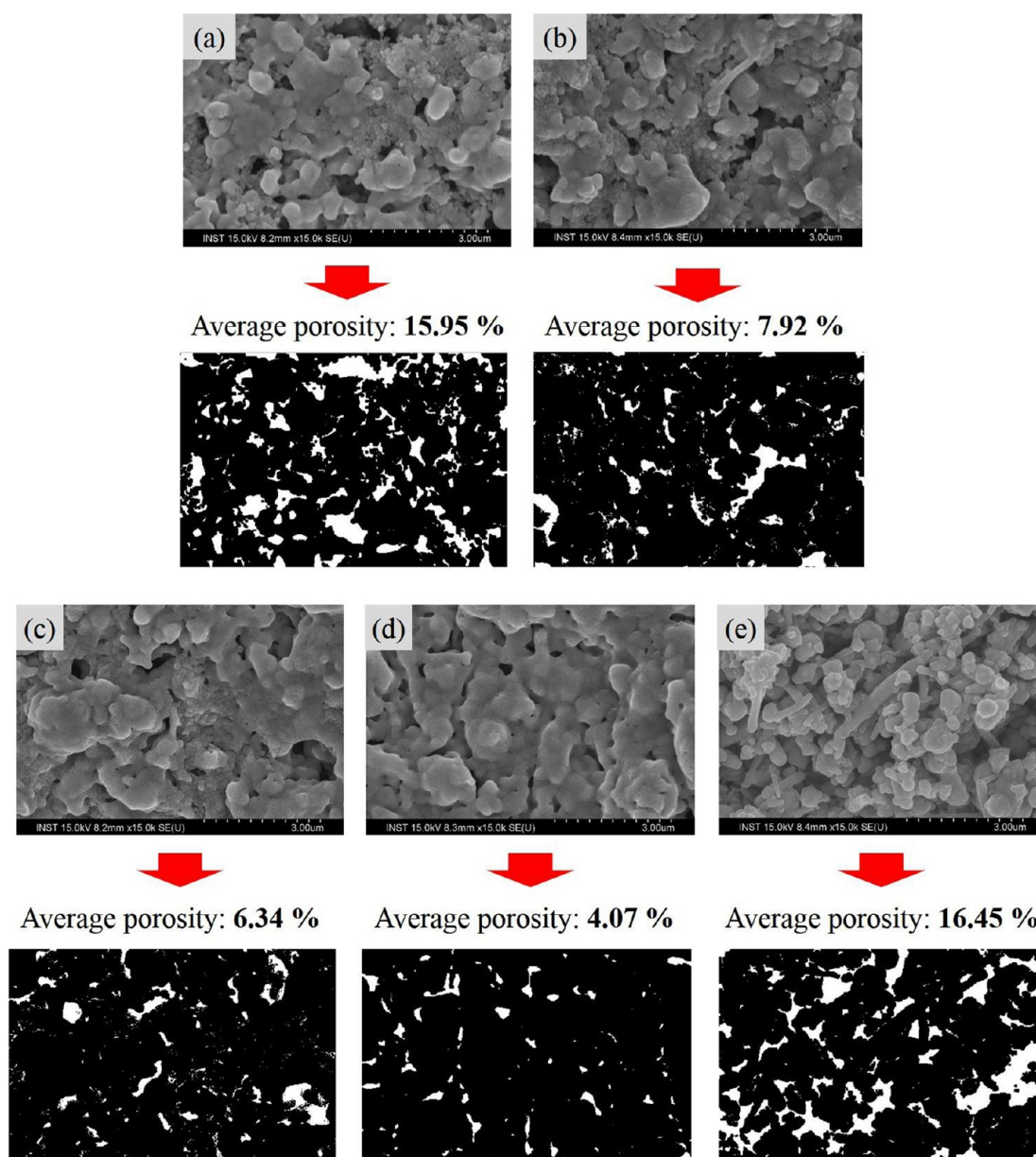


Figure 7. Calculated average porosity of the flash light-sintered Cu NW/NP ink film using low-resolution SEM images: (a) 0, (b) 1, (c) 3, (d) 5, and (e) 100 wt % of Cu NWs (irradiation energy: $12.5 \text{ J}\cdot\text{cm}^{-2}$, pulse duration: 10 ms, pulse number: 1).

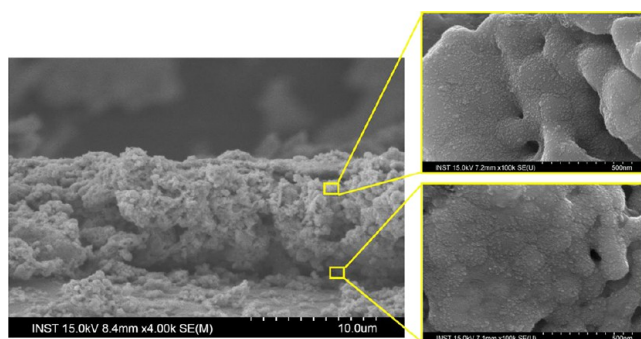


Figure 8. Cross-sectional morphology of the flash light-sintered Cu NW/NP ink film. (insets) High-resolution SEM images of upper part (upper) and bottom part (lower) of the flash light-sintered Cu NW/NP ink film (irradiation energy: $12.5 \text{ J}\cdot\text{cm}^{-2}$, pulse duration: 10 ms, pulse number: 1).

318 °C, allowing the complete vaporization of the PVP and fully melting the Cu NPs. Subsequently, the melted liquid Cu NPs were agglomerated and enlarged with solidifying procedure.³³

In conclusion, an irradiation energy of $12.5 \text{ J}\cdot\text{cm}^{-2}$ with one pulse and a 10 ms duration was determined as the optimal flash light-sintering condition for all of the Cu NW wt % specimens.

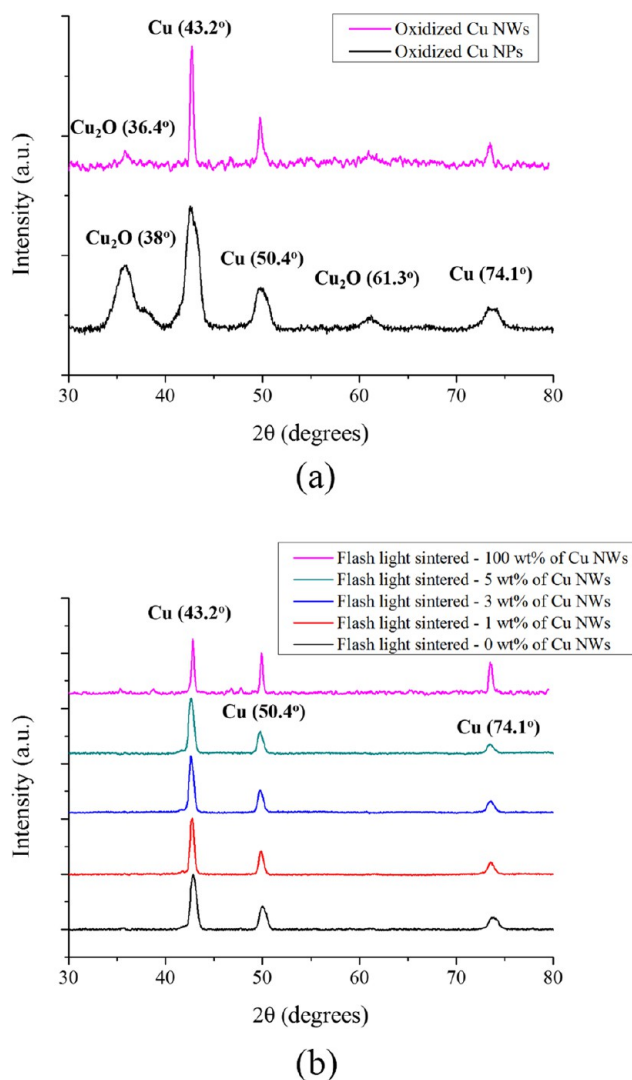


Figure 9. X-ray diffraction patterns of Cu NW/NP ink film for (a) unsintered and (b) flash light-sintered cases (irradiation energy: $12.5 \text{ J}\cdot\text{cm}^{-2}$, pulse duration: 10 ms, pulse number: 1).

In the flash light-sintering condition of $12.5 \text{ J}\cdot\text{cm}^{-2}$ energy, the sheet resistance of the sintered Cu NW/NP ink decreased as the wt % of Cu NWs increased to 5 wt %. However, the 100 wt % of Cu NWs case showed the highest sheet resistance among all the wt % cases. Accordingly, the 5 wt % Cu NW case showed a sheet resistance of $21 \text{ m}\Omega\cdot\text{cm}^{-1}$, which is lower than those of any other cases.

To measure the thicknesses of the Cu NW/NP ink films, surface profiling analysis using an α -step instrument was conducted (Figure 5). The cross-sectional profiles were measured from a to a' (unsintered case) and from b to b' ($12.5 \text{ J}\cdot\text{cm}^{-2}$ flash light-sintered case), as shown in Figure 5a. The thickness of the unsintered Cu NW/NP ink film was $14.87 \mu\text{m}$ (Figure 5b). Meanwhile, the thickness of the Cu NW/NP ink films decreased to $\sim 10 \mu\text{m}$ after the $12.5 \text{ J}\cdot\text{cm}^{-2}$ flash light-sintering process (Figures 5c–g). Using these results, the resistivity of the Cu NW/NP ink film was calculated using the measured sheet resistance, as shown in Table 3. It was found that the resistivity of the Cu NW/NP ink film decreased as the wt % of Cu NWs increased. The $12.5 \text{ J}\cdot\text{cm}^{-2}$ flash light-sintered Cu NW/NP ink film with 5 wt % Cu NW showed the lowest resistivity of

$22.77 \mu\Omega\cdot\text{cm}$, which is 12.87 times higher than the resistivity of bulk Cu ($1.77 \mu\Omega\cdot\text{cm}$, see Table 3).

To investigate the morphologies of the $12.5 \text{ J}\cdot\text{cm}^{-2}$ flash light-sintered Cu NW/NP ink films with respect to the wt % of Cu NWs, SEM images were obtained. As shown in Figure 6a,e, necking among the pure Cu NPs and Cu NWs, respectively, was observed. These structures have high porosity between Cu NPs and Cu NWs after flash light-sintering process, resulting in high resistivity.² Meanwhile, the 1, 3, and 5 wt % Cu NWs cases showed a tangled mixture of Cu NWs and Cu NPs (Figure 6b–d). It was also found that the Cu NPs were melted and firmly welded onto the Cu NWs. The network structures with the highly tangled Cu NPs and Cu NWs appear to be more dense as the wt % Cu NWs increased to 5 wt % (Figure 6). This result also could be seen in average porosity calculation result. As shown in Figure 7, the porosity of flash light-sintered Cu NW/NP ink films was decreased as the wt % of Cu NWs increased to 5 wt %. It is noteworthy that the 0 and 100 wt % Cu NW cases showed the high average porosity (15.95% and 16.45%, respectively), whereas that of 5 wt % Cu NWs case was 4.07%. Accordingly, higher electrical conductivity at 5 wt % Cu NW/NP ink film than those of 1 and 3 wt % Cu NW/NP ink films was attributed to the densely packed network of Cu NW/NP structure (Table 3). In the cases of only Cu NPs and Cu NWs, the electrons moved along a zigzag path through the necklike junction. Meanwhile, the flash light-sintered Cu NW/NP structure provided the quickest way for the electrons to move, which results in a high electrical conductivity.²⁷ Furthermore, to investigate the sintering state of $12.5 \text{ J}\cdot\text{cm}^{-2}$ flash light-sintered Cu NW/NP ink films, the cross-sectional morphology was taken as shown in Figure 8. As a result, the bottom part of the flash light-sintered Cu NW/NP ink film as well as the upper part of one was fully sintered. From these experiments, it is concluded that the 5 wt % of Cu NWs with $12.5 \text{ J}\cdot\text{cm}^{-2}$ irradiation energy is the optimized condition of flash light sintering.

Figure 9 shows the XRD results used to investigate the crystal phase of the unsintered and flash light-sintered Cu NW/NP ink films. The XRD patterns of raw materials of Cu NPs and Cu NWs showed peaks at 36.4° , 38° , and 61.3° , corresponding to Cu₂O and CuO, respectively, as they were covered with Cu oxides (Figure 9a). After flash light sintering at $12.5 \text{ J}\cdot\text{cm}^{-2}$, complete removal of the Cu oxide peaks was observed, and the intensity of the Cu phase peaks (43.2° , 50.4° , and 74.1°) increased, which is evidence of the complete reduction and sintering of the Cu NW/NP ink films (Figure 9b). It is noteworthy that the flash light irradiation completely reduced the oxide shells covering not only the Cu NPs but also the Cu NWs to pure copper.

To investigate the reliability of the flash light-sintered Cu NPs ink films, outer bending tests were performed as a function of the bending radius. For these tests, the resistance change ($\Delta R\cdot R_0^{-1}$) was expressed as follows:

$$\Delta R\cdot R_0^{-1} = (R - R_0)\cdot R_0^{-1} \quad (2)$$

where R is the measured resistance after the bending test, and R_0 is the initial resistance. The R values were measured every 100 cycles. Figure 10 shows the $\Delta R\cdot R_0^{-1}$ results obtained during the repeated outer bending fatigue test in the case of 0 wt % Cu NWs. The $\Delta R\cdot R_0^{-1}$ value increased as the cycle number increased because crack initiation and propagation occurred in the Cu NPs ink film due to the repeated tensile loading. As shown in Figure 10a, the $\Delta R\cdot R_0^{-1}$ value gradually increased to 600 cycles because of crack initiation and generation in the Cu NP ink film, as observed in the SEM images in Figures 10b,c. After 600 cycles, the $\Delta R\cdot R_0^{-1}$ value drastically increased due to the acceleration of

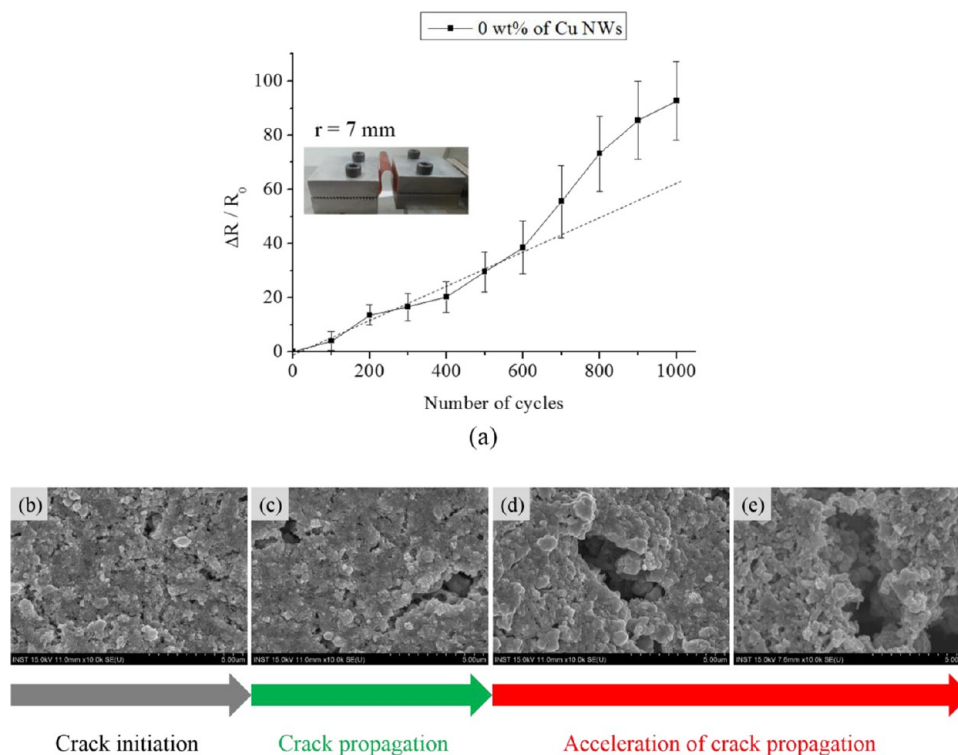


Figure 10. Outer bending fatigue test results about (a) bending radius of $r = 7$ mm and SEM images of the fatigue-tested Cu NPs ink film after (b) 400, (c) 600, (d) 800, and (e) 1000 cycles of bending.

crack propagation and its rapid growth³⁶ (Figures 10d,e), resulting from weakened necklike junctions among the Cu NPs due to repeated tensile loading. For this reason, large cracks were formed among the flash light-sintered Cu NPs and propagated easily during the outer bending. As a result, the $\Delta R \cdot R_0^{-1}$ value of the 0 wt % Cu NWs case after 1000 cycles was 92.75.

The bending fatigue tests of the $12.5 \text{ J} \cdot \text{cm}^{-2}$ flash light-sintered Cu NW/NP inks were performed while varying the bending radius to 7, 10, and 15 mm. Figure 11 shows the $\Delta R \cdot R_0^{-1}$ results obtained in the repeated outer bending fatigue tests. As shown in Figure 11a, the $\Delta R \cdot R_0^{-1}$ values decreased when even only 1 wt % Cu NWs was added, as shown in Figure 11a (the red line). As a result, the $\Delta R \cdot R_0^{-1}$ value of the 1 wt % Cu NWs case was 20.57 after 1000 cycles, which is 4.5 times lower than that of the 0 wt % Cu NW case (92.75). The $\Delta R \cdot R_0^{-1}$ values of the 3, 5, and 100 wt % Cu NW cases were 5.23, 4.19, and 3.65, respectively, with no crack acceleration occurring during the fatigue tests (Figure 11a; the green, blue, and pink lines).

As part of the in-depth study of these phenomena, SEM images of the flash light-sintered Cu NW/NP ink films were obtained (Figures 11d–h) after 1000 cycles of outer bending tests. In the outer bending testing of the 0 wt % Cu NWs, a large crack attributed to the acceleration of crack propagation was found among the Cu NPs and Cu NWs, as mentioned above (Figure 10). Meanwhile, the influence of the Cu NWs was clearly observed as the wt % of Cu NWs increased. As shown in Figure 11e, the size of the crack among the Cu NPs decreased because the Cu NWs prevented necklike junctions and subsequent crack initiation and retarded crack propagation under the tensile loading. As the wt % of Cu NWs increased, this phenomenon was more clearly observed over the entire Cu NW/NP ink film, as shown in Figure 11e–h. The 5 and 100 wt % Cu NWs showed only a few small cracks (Figure 11g,h). This phenomenon is also strongly related to the density of the flash light-sintered Cu NW/NP-ink

films because the ductility of Cu material is proportional to the density of film: the nanocrystalline Cu with the grain size under 25 nm has ductility under 2%. On the other hand, the bulk Cu has much larger ductility, up to 70% elongation.^{23,24} Therefore, it is difficult for 0 wt % Cu NWs case as well as the nanocrystalline Cu to endure under repeatable tensile condition due to the highly concentrated stress at small necklike junctions, resulting in brittle fracture of film. Meanwhile, in the case of 5 wt % Cu NWs, the Cu NWs supplemented the density of film in Cu NPs porous media, thereby resulting in much higher durability under repeatable bending conditions. Also, the NWs have unique properties such as high flexibility and stretchability due to its wire-shaped structure.^{20,37,38} Therefore, the Cu NWs contributed to densification and flexibility of film. Accordingly, the mechanical performance of flash light-sintered Cu NW/NP ink films under fatigue condition was greatly improved as the wt % of the Cu NWs increased. Meanwhile, in the case of 100 wt % Cu NWs, Cu film consisting of only Cu NWs have excellent mechanical flexibility and stretchability, which make it possible to sustain the electrical conductivity in spite of the highest porous structure among all the cases (Figure 11h).^{20,37–39}

In the same manner, in the cases of bending radii of 10 mm and 15 mm, the $\Delta R \cdot R_0^{-1}$ values after 1000 cycles of outer bending decreased as the wt % of Cu NWs increased, similar to the case of the 7 mm bending radius. It is noteworthy that abrupt crack accelerations did not occur in the 3, 5, and 100 wt % cases but occurred in the 0 and 1 wt % Cu NWs cases, as shown in Figure 11b,c. Again, this demonstrates the role of Cu NWs in retarding crack propagation. Also, the Cu NWs strengthen the weakest part of the porous structure of sintered Cu NPs with distributing the stress from necking area of Cu NPs to Cu NWs,⁴⁰ resulting in improving their mechanical properties under repeatable tensile loading. Therefore, it was concluded that randomly dispersed Cu NWs, welded among the sintered Cu

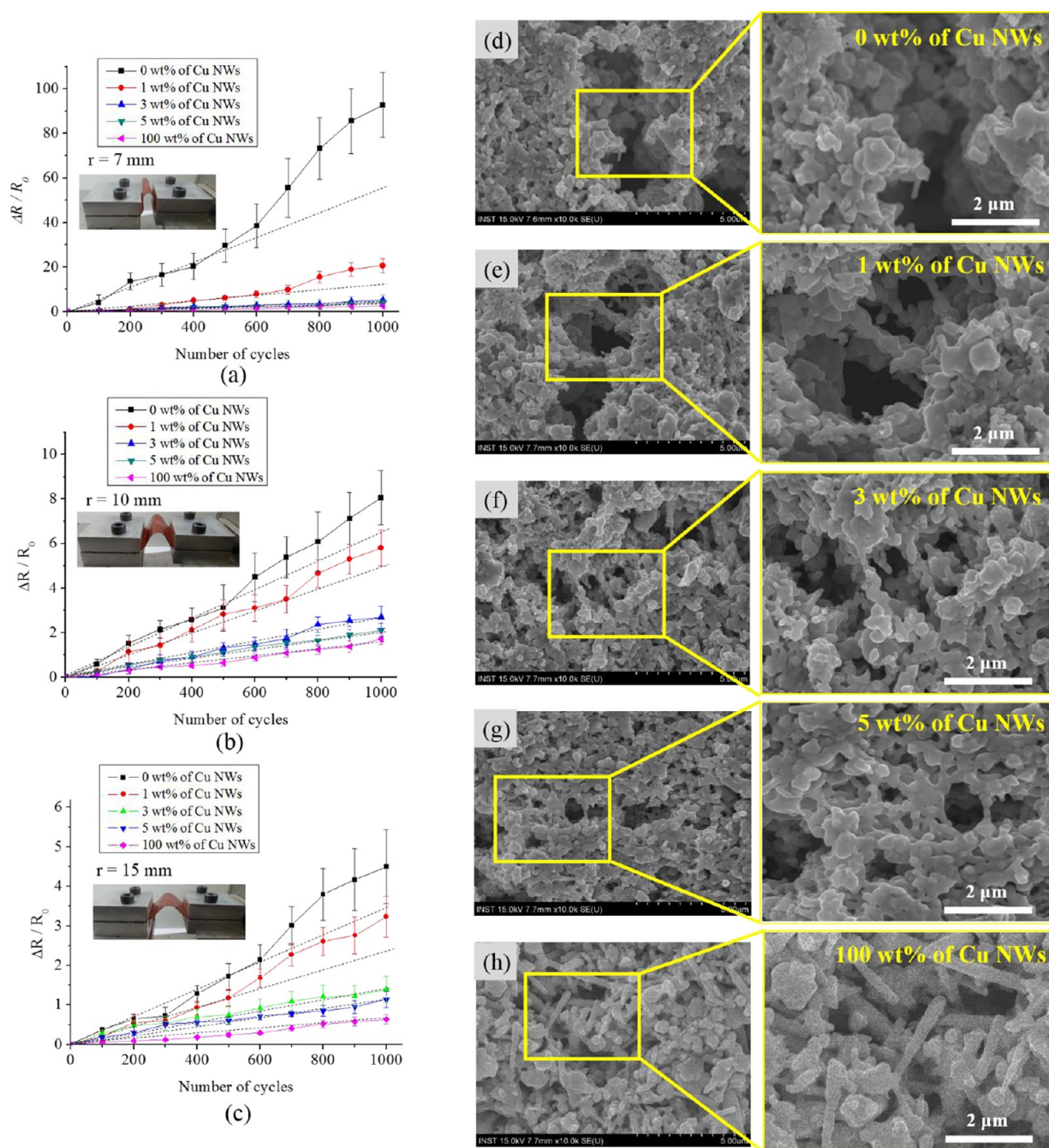


Figure 11. Outer bending fatigue test results about bending radius of (a) $r = 7$ mm, (b) $r = 10$ mm, and (c) $r = 15$ mm. (insets) Photographs of the specimen for outer bending fatigue test with respect to the bending radius. SEM images of the fatigue-tested Cu NW/NP ink film: the 1000 cycles of outer bending fatigue test results of (d) 0, (e) 1, (f) 3, (g) 5, and (h) 100 wt % of Cu NWs.

NPs, can enhance the reliability of Cu NW/NP ink film under tensile loading, as expressed in the schematic of Figure 13.

Figure 12 shows the inner bending fatigue test results of the Cu NW/NP ink films. As shown in Figure 12a, in the 0 wt % Cu NW cases, the $\Delta R \cdot R_0^{-1}$ value gradually increased through 600 cycles and then drastically increased due to acceleration of crack propagation. The $\Delta R \cdot R_0^{-1}$ value of this 0 wt % case was 84.03 after 1000 cycles (black line in Figure 12a). Meanwhile, those after 1, 3, 5, and 100 wt % Cu NW cases after 1000 cycles were 14.88, 4.94, 3.72, and 2.66, respectively, as demonstrated in Figure 12a (the red, green, blue, and pink lines). In particular, the 3, 5, and 100 wt % Cu NW cases showed no crack acceleration during the fatigue tests, indicating that the Cu NWs prevent crack initiation

and propagation due to compressive loading. Figure 12d shows the 0 wt % Cu NWs case after 1000 cycles of the inner bending fatigue test. Similar to the outer bending test case (Figure 11), a large crack due to compressive loading was observed. The cracks among the Cu NPs decreased as the wt % of Cu NWs increased, as seen in Figure 12d–h, because the Cu NWs enhanced the mechanical reliability of the Cu NW/NP ink films.^{41,42} As a result, the 5 and 100 wt % Cu NWs cases showed only a few small cracks compared to the lower wt % Cu NW cases. This is because of the high density and flexibility of Cu NW/NP ink films with 5 wt % Cu NWs and the enhanced fatigue characteristics due to the highly flexible film of 100 wt % Cu NWs under compressive condition, as mentioned in outer bending test. In the same

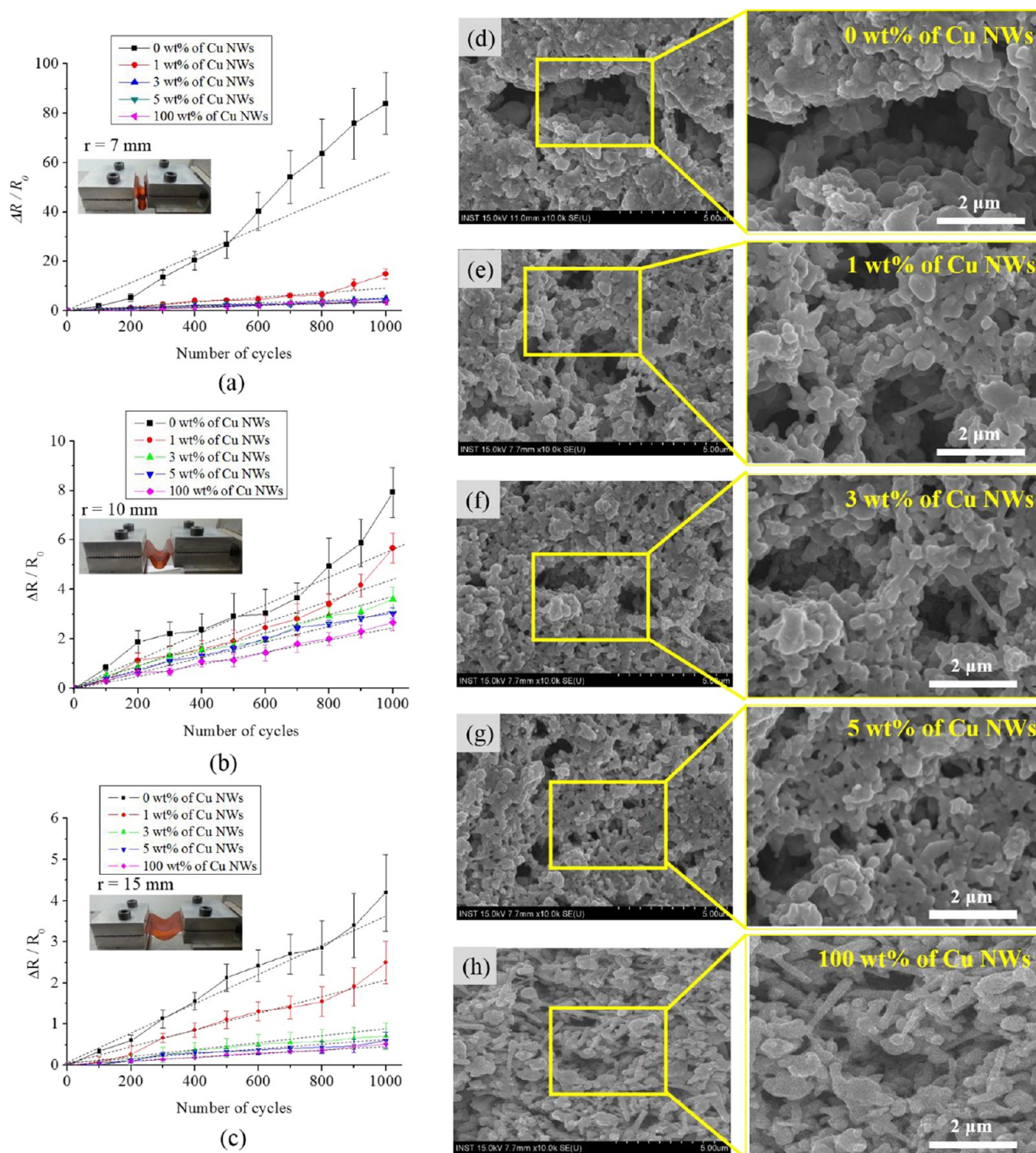


Figure 12. Inner bending fatigue test results about bending radius of $r =$ (a) 7, (b) 10, and (c) 15 mm. (insets) Photographs of the specimen for inner bending fatigue test with respect to the bending radius. SEM images of the fatigue-tested Cu NW/NP ink film: the 1000 cycles of inner bending fatigue test results of (d) 0, (e) 1, (f) 3, (g) 5, and (h) 100 wt % of Cu NWs.

manner, acceleration of the changes of $\Delta R \cdot R_0^{-1}$ due to inner bending fatigue was prevented in the 3, 5, and 100 wt % Cu NW cases (Figure 12a–c). The $\Delta R \cdot R_0^{-1}$ value increased as the bending radius decreased where the $\Delta R \cdot R_0^{-1}$ values after 1000 cycles of the inner bending fatigue test with bending radii of 7, 10, and 15 mm were 2.66, 1.72, and 0.49, respectively. Therefore, it was concluded that the addition of more than 3 wt % Cu NWs into Cu NP ink can efficiently prevent crack generation and propagation caused by inner and outer bending loading (see Figure 12). However, the 100 wt % Cu NW case showed high resistivity due to its porous structures after flash light sintering and the highest mechanical reliability under

repeatable tensile and compression loading conditions. Meanwhile, the 5 wt % Cu NWs case showed remarkably low resistivity with enhanced fatigue characteristics, which is comparable to 100 wt % of Cu NWs. As a result, this addition can greatly enhance the reliability of flexible electrodes in printed electronics applications (Figure 13).

CONCLUSION

In this work, the effects of Cu NWs on the reliability of a flash light-sintered Cu NP/NW printed electrodes were investigated under repeatable outer and inner bending fatigue loading. The $\Delta R \cdot R_0^{-1}$ values after fatigue test decreased significantly in the case

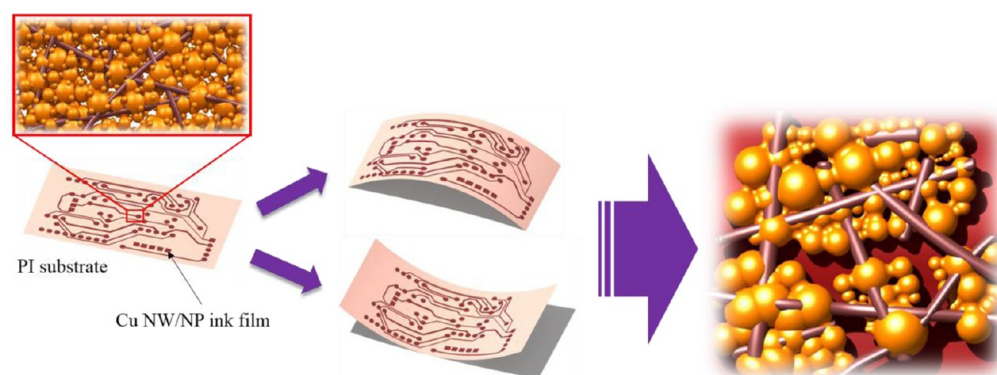


Figure 13. A schematic illustration of the improved reliability of flash light-sintered Cu NW/NP ink film under outer bending (tension) and inner bending (compression) conditions.

of 5 wt % Cu NWs because the Cu NWs supplemented the density and mechanical flexibility of film, which retarded crack initiation and propagation. Furthermore, the flash light-sintered Cu NW/NP ink films showed a lower resistivity than that of the Cu NPs ink films with a value of $22.77 \mu\Omega\text{-cm}$ for the 5 wt % Cu NWs case compared to $94.01 \mu\Omega\text{-cm}$ and $104.15 \mu\Omega\text{-cm}$ for the cases of pure Cu NPs and Cu NWs. It is expected that the results obtained in this work can be widely used to enhance the reliability under bending of flexible electronic circuits.

AUTHOR INFORMATION

Corresponding Author

*Phone: 82-2-2220-2898. E-mail: kima@hanyang.ac.kr.

Notes

The authors declare no competing financial interest.

ACKNOWLEDGMENTS

This research was supported by the Basic Science Research Program through the National Research Foundation of Korea (NRF) funded by the Ministry of Education (2012R1A6A1029029). This work was supported by a National Research Foundation of Korea (NRF) grant funded by the Korean Government (MEST) (No. 2013M2A2A9043280). We would like to acknowledge the financial support from the R&D Convergence Program of MSIP (Ministry of Science, ICT, and Future Planning) and ISTK (Korea Research Council for Industrial Science and Technology) of the Republic of Korea (Grant B551179-13-02-05). This work was also supported by the Technology Innovation Program (or Industrial Strategic Technology Development Program, 10048913, Development of the cheap nanoink, which is sintered in the air for smart devices) funded by the Ministry of Trade, Industry, & Energy (MI, Korea).

REFERENCES

- (1) Dharmadasa, R.; Jha, M.; Amos, D. A.; Druffel, T. Room Temperature Synthesis of a Copper Ink for the Intense Pulsed Light Sintering of Conductive Copper Films. *ACS Appl. Mater. Interfaces* **2013**, *5* (24), 13227–13234.
- (2) Kang, H.; Sowade, E.; Baumann, R. R. Direct Intense Pulsed Light Sintering of Inkjet-Printed Copper Oxide Layers within Six Milliseconds. *ACS Appl. Mater. Interfaces* **2014**, *6* (3), 1682–1687.
- (3) Xu, P. Y.; Hamilton, M. C. Reduced-Loss Ink-Jet Printed Flexible CPW With Copper Coating. *IEEE Microwave Wireless Compon. Lett.* **2013**, *23* (4), 178–180.
- (4) Li, D. P.; Sutton, D.; Burgess, A.; Graham, D.; Calvert, P. D. Conductive copper and nickel lines via reactive inkjet printing. *J. Mater. Chem.* **2009**, *19* (22), 3719–3724.
- (5) Perelaer, J.; Schubert, U. S. Novel approaches for low temperature sintering of inkjet-printed inorganic nanoparticles for roll-to-roll (R2R) applications. *J. Mater. Res.* **2013**, *28* (4), 564–573.
- (6) Ishizaki, M.; Kanaizuka, K.; Abe, M.; Hoshi, Y.; Sakamoto, M.; Kawamoto, T.; Tanaka, H.; Kurihara, M. Preparation of electrochromic Prussian blue nanoparticles dispersible into various solvents for realisation of printed electronics. *Green Chem.* **2012**, *14* (5), 1537–1544.
- (7) Cheng, Z. P.; Zhong, H.; Xu, J. M.; Chu, X. Z.; Song, Y. Z.; Xu, M.; Huang, H. Facile fabrication of ultrasmall and uniform copper nanoparticles. *Mater. Lett.* **2011**, *65* (19–20), 3005–3008.
- (8) Shin, D. H.; Woo, S.; Yem, H.; Cha, M.; Cho, S.; Kang, M.; Jeong, S.; Kim, Y.; Kang, K.; Piao, Y. A Self-Reducible and Alcohol-Soluble Copper-Based Metal-Organic Decomposition Ink for Printed Electronics. *ACS Appl. Mater. Interfaces* **2014**, *6* (5), 3312–3319.
- (9) Kim, Y.; Lee, B.; Yang, S.; Byun, I.; Jeong, L.; Cho, S. M. Use of copper ink for fabricating conductive electrodes and RFID antenna tags by screen printing. *Curr. Appl. Phys.* **2012**, *12* (2), 473–478.
- (10) Wang, B. Y.; Yoo, T. H.; Song, Y. W.; Lim, D. S.; Oh, Y. J. Cu Ion Ink for a Flexible Substrate and Highly Conductive Patterning by Intensive Pulsed Light Sintering. *ACS Appl. Mater. Interfaces* **2013**, *5* (10), 4113–4119.
- (11) Zenou, M.; Ermak, O.; Saar, A.; Kotler, Z. Laser sintering of copper nanoparticles. *J. Phys. D: Appl. Phys.* **2014**, *47*, 2.
- (12) Lee, J.; Lee, B.; Jeong, S.; Kim, Y.; Lee, M. Microstructure and electrical property of laser-sintered Cu complex ink. *Appl. Surf. Sci.* **2014**, *307*, 42–45.
- (13) Ko, H.; Jhin, J.; Byun, D.; Lee, J.; Park, D. Copper thin films on PET prepared at ambient temperature by ECR-CVD. *IEEE Trans. Compon. Packag. Technol.* **2005**, *28* (4), 781–784.
- (14) Joo, M.; Lee, B.; Jeong, S.; Lee, M. Comparative studies on thermal and laser sintering for highly conductive Cu films printable on plastic substrate. *Thin Solid Films* **2012**, *520* (7), 2878–2883.
- (15) Perelaer, J.; de Gans, B. J.; Schubert, U. S. Ink-jet printing and microwave sintering of conductive silver tracks. *Adv. Mater.* **2006**, *18* (16), 2101–2104.
- (16) Kim, H. S.; Dhage, S. R.; Shim, D. E.; Hahn, H. T. Intense pulsed light sintering of copper nanoink for printed electronics. *Appl. Phys. A: Mater. Sci. Process.* **2009**, *97* (4), 791–798.
- (17) Ryu, J.; Kim, H. S.; Hahn, H. T. Reactive Sintering of Copper Nanoparticles Using Intense Pulsed Light for Printed Electronics. *J. Electron. Mater.* **2011**, *40* (1), 42–50.
- (18) Han, W. S.; Hong, J. M.; Kim, H. S.; Song, Y. W. Multi-pulsed white light sintering of printed Cu nanoinks. *Nanotechnology* **2011**, *22*, 39.
- (19) Hwang, H. J.; Chung, W. H.; Kim, H. S. In situ monitoring of flash-light sintering of copper nanoparticle ink for printed electronics. *Nanotechnology* **2012**, *23*, 48.

- (20) Hu, W.; Wang, R.; Lu, Y.; Pei, Q. An elastomeric transparent composite electrode based on copper nanowires and polyurethane. *J. Mater. Chem. C* **2014**, *2* (7), 1298–1305.
- (21) Sekitani, T.; Someya, T. Stretchable, Large-area Organic Electronics. *Adv. Mater.* **2010**, *22* (20), 2228–2246.
- (22) Siow, K. S. Mechanical properties of nano-silver joints as die attach materials. *J. Alloys Compd.* **2012**, *514*, 6–19.
- (23) Koch, C. C.; Morris, D. G.; Lu, K.; Inoue, A. Ductility of nanostructured materials. *MRS Bull.* **1999**, *24* (2), 54–58.
- (24) Youssef, K. M.; Scattergood, R. O.; Murty, K. L.; Horton, J. A.; Koch, C. C. Ultrahigh strength and high ductility of bulk nanocrystalline copper. *Appl. Phys. Lett.* **2005**, *87* (9).
- (25) Laha, T.; Chen, Y.; Lahiri, D.; Agarwal, A. Tensile properties of carbon nanotube reinforced aluminum nanocomposite fabricated by plasma spray forming. *Composites, Part A* **2009**, *40* (5), 589–594.
- (26) Yoon, T.; Shin, W. C.; Kim, T. Y.; Mun, J. H.; Kim, T. S.; Cho, B. J. Direct Measurement of Adhesion Energy of Monolayer Graphene As-Grown on Copper and Its Application to Renewable Transfer Process. *Nano Lett.* **2012**, *12* (3), 1448–1452.
- (27) Lee, I.; Lee, J.; Ko, S. H.; Kim, T. S. Reinforcing Ag nanoparticle thin films with very long Ag nanowires. *Nanotechnology* **2013**, *24* (41).
- (28) Cheng, S.; Spencer, J.; Milligan, W. Strength and tension/compression asymmetry in nanostructured and ultrafine-grain metals. *Acta Mater.* **2003**, *51* (15), 4505–4518.
- (29) Chung, W. H.; Hwang, H. J.; Lee, S. H.; Kim, H. S., In situ monitoring of a flash light sintering process using silver nano-ink for producing flexible electronics. *Nanotechnology* **2013**, *24* (3).
- (30) Park, S. I.; Ahn, J. H.; Feng, X.; Wang, S. D.; Huang, Y. G.; Rogers, J. A. Theoretical and Experimental Studies of Bending of Inorganic Electronic Materials on Plastic Substrates. *Adv. Funct. Mater.* **2008**, *18* (18), 2673–2684.
- (31) Cho, C. K.; Hwang, W. J.; Eun, K.; Choa, S. H.; Na, S. I.; Kim, H. K. Mechanical flexibility of transparent PEDOT:PSS electrodes prepared by gravure printing for flexible organic solar cells. *Sol. Energ. Mater. Sol. Cells* **2011**, *95* (12), 3269–3275.
- (32) Lo, C.; Chou, K.-S.; Chin, W.-K. Effects of mixing procedures on the volume fraction of silver particles in conductive adhesives. *J. Adhes. Sci. Technol.* **2001**, *15* (7), 783–792.
- (33) Park, S. H.; Chung, W. H.; Kim, H. S. Temperature changes of copper nanoparticle ink during flash light sintering. *J. Mater. Process. Technol.* **2014**, *214* (11), 2730–2738.
- (34) Joo, S. J.; Hwang, H. J.; Kim, H. S. Highly conductive copper nano/microparticles ink via flash light sintering for printed electronics. *Nanotechnology* **2014**, *25* (26), 265601.
- (35) Kim, Y.-J.; Ryu, C.-H.; Park, S.-H.; Kim, H.-S. The effect of poly (N-vinylpyrrolidone) molecular weight on flash light sintering of copper nanopaste. *Thin Solid Films* **2014**, *570*, 114–122.
- (36) Kim, B. J.; Cho, Y.; Jung, M. S.; Shin, H. A.; Moon, M. W.; Han, H. N.; Nam, K. T.; Joo, Y. C.; Choi, I. S. Fatigue-Free, Electrically Reliable Copper Electrode with Nanohole Array. *Small* **2012**, *8* (21), 3300–3306.
- (37) Cheng, Y.; Wang, S.; Wang, R.; Sun, J.; Gao, L. Copper nanowire based transparent conductive films with high stability and superior stretchability. *J. Mater. Chem. C* **2014**, *2* (27), 5309–5316 DOI: 10.1039/C4TC00375F.
- (38) Song, J.; Li, J.; Xu, J.; Zeng, H. Superstable Transparent Conductive Cu@Cu₄Ni Nanowire Elastomer Composites against Oxidation, Bending, Stretching, and Twisting for Flexible and Stretchable Optoelectronics. *Nano Lett.* **2014**, *14* (11), 6298–6305.
- (39) Wang, J.; Yan, C.; Lin, M.-F.; Tsukagoshi, K.; Lee, P. S. Solution-assembled nanowires for high performance flexible and transparent solar-blind photodetectors. *J. Mater. Chem. C* **2015**, *3* (3), 596–600.
- (40) Ye, H.; Lam, H.; Titchenal, N.; Gogotsi, Y.; Ko, F. Reinforcement and rupture behavior of carbon nanotubes–polymer nanofibers. *Appl. Phys. Lett.* **2004**, *85* (10), 1775–1777.
- (41) Ye, S. R.; Rathmell, A. R.; Stewart, I. E.; Ha, Y. C.; Wilson, A. R.; Chen, Z. F.; Wiley, B. J. A rapid synthesis of high aspect ratio copper nanowires for high-performance transparent conducting films. *Chem. Commun.* **2014**, *50* (20), 2562–2564.
- (42) Wang, S. L.; Cheng, Y.; Wang, R. R.; Sun, J.; Gao, L. Highly Thermal Conductive Copper Nanowire Composites with Ultralow Loading: Toward Applications as Thermal Interface Materials. *ACS Appl. Mater. Interfaces* **2014**, *6* (9), 6481–6486.